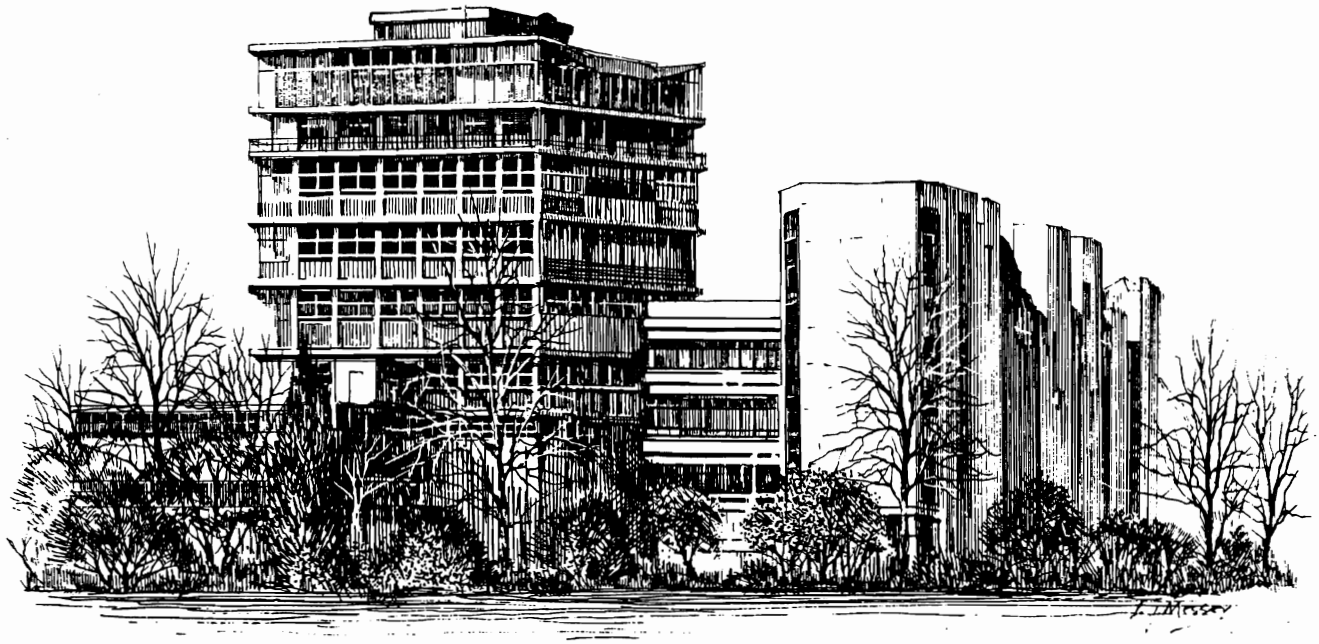
UNIVERSITY OF OXFORD

Department of Engineering Science

Parks Road

Oxford

REPORT



2296/07

The Design of a a Fast Orbit Beam Stabilisation System for the Diamond Synchrotron

Stephen Duncan,
Department of Engineering Science,
University of Oxford,
Oxford OX1 3PJ, United Kingdom

August 2007

Summary

1. This report concludes that the controller should take the form

$$\mathbf{C}(z^{-1}) = c(z^{-1})\mathbf{C}$$

where

$$\mathbf{C} = \mathbf{V}\mathbf{D}\mathbf{\Sigma}^{-1}\mathbf{U}_1^{\mathrm{T}}$$

with $\mathbf{V}$ and $\mathbf{U}_1$ being derived from the singular value decomposition of the steady state response matrix $\mathbf{B} = \mathbf{U}_1\mathbf{\Sigma}\mathbf{V}^{\mathrm{T}}$ where $\mathbf{\Sigma} = \mathrm{diag}\{\sigma_n\}$, and $\mathbf{D} = \mathrm{diag}\{d_n\}$ with

$$d_n = \frac{\sigma_n^2}{\sigma_n^2 + \mu}$$

This structure means that only one matrix multiplication is required when generating the actuator inputs. Since σ_n and d_n are small as n becomes large, the diagonal elements of both $\mathbf{D}$ and $\mathbf{\Sigma}^{-1}$ should both be set to zero for $n > 71$, to avoid the effect of these small gains of the higher order modes being amplified by the integral action in the controller dynamics.

2. The controller dynamics are based on an Internal Model design and take the form

$$c(z^{-1}) = \frac{(1-\lambda)}{(b_0+b_1)}\frac{1-a_1z^{-1}}{1-\lambda z^{-1}-(1-\lambda)z^{-d}\beta(z^{-1})}$$

where a_1, b_0 and b_1 are the parameters of the discrete time response of a sample and hold model of the actuators with sample period T, and d denotes the time delay (expressed in number of samples) in applying the control action, with

$$\beta(z^{-1}) = \frac{b_0+b_1z^{-1}}{(b_0+b_1)}$$

and $\lambda = \mathrm{e}^{-\zeta T}$ where ζ is the closed loop bandwidth (in rad.s^{-1}) of the controller. The same controller dynamics are applied to each spatial mode, with the dynamics being de-tuned by the controller gains, d_n. The denominator of $c(z^{-1})$ contains a root at $z = 1$, so the controller includes integral action.

3. For an example data set containing 10s of the horizontal disturbances recorded at each of the sensors, most of the power is concentrated in the low frequency end of the first 10 modes, with the major frequency component of the disturbance occurring at 25Hz. Choosing $\zeta = 2\pi.400$ rad.s^{-1} gives a closed loop bandwidth of 400Hz, which leads to controller dynamics of the form

$$c(z^{-1}) = \frac{1.005 - 0.944z^{-1}}{1 - 0.7778z^{-1} - 0.1548z^{-4} - 0.0674z^{-5}}$$

Setting $\mu = {\sigma_5}^2$ focusses the control action in these lower order modes and the controller attenuates disturbances at 25Hz by at least 6dB for the first 10 modes.

4. The control dynamics include integral action, so steady state errors will be removed and the controller will attenuate disturbances at 0.1Hz up to the 71st mode.

5. The controller has a gain margin of 3.53 and a phase margin of 69.7°. The system will remain stable in the presence of errors in the steady state response matrix of the actuators, provided that $\|\mathbf{E}\|_2 < 2\sqrt{\mu}\gamma$, where the true response is $\tilde{\mathbf{B}} = \mathbf{B} + \mathbf{E}$ and γ is the minimum distance from the $-1 + \mathrm{j}0$ point to the Nyquist plot associated with the open loop response of the first mode. When $\mu = {\sigma_5}^2$, this corresponds to requiring that $\|\mathbf{E}\|_2 < 35.0$. Given that $\|\mathbf{B}\|_2 = 146.1$, this represents a 24.0% fractional error in the norm of the steady state matrix. This needs to be checked against an estimate of $\|\mathbf{E}\|_2$ from the norm of the difference between the measured steady state response and the response matrix obtained from modelling.

6. The controller reduces the standard deviation of the variation observed at all sensors by (on average) 46%, which for the example disturbance used as the basis of the design, reduces the average standard deviation from 2.8μm without control to 1.2μm when control is applied.

7. It would be possible to reduce the variation further by increasing the closed loop bandwidth ζ and/or decreasing μ so that control is extended to higher order modes. However, this will result in a controller that is more sensitive to modelling errors and may lead to instability.

8. The controller dynamics could be replaced by a PI controller, which has a similar closed loop bandwidth, but is less robust to modelling errors. The IMC controller is the preferable solution given that it does not require significantly more computation to implement.

9. Currently, the control law attempts to apply the same level of control to the variation in each sensor. However, there are considerable differences between the levels of disturbance observed at different sensors and it would be possible to allow for this in the control design by including a weighting matrix in $\mathbf{C}$ so that the control focusses on sensors that have the largest variation and/or on sensors where minimizing the deviation is most important (*e.g.* immediately before a beam extraction point). This extension has not been considered in the design presented here.

1 Introduction

Synchrotrons can produce very intense of X-rays and ultra violet light for a range of applications including protein crystallography, materials characterisation and high resolution imaging. The Diamond Light Source is a recently constructed synchrotron that produces a 3GeV electron beam in a ring of circumference 560m. A key component of the process is the fast beam stabilisation system that regulates the horizontal and vertical position of the beam in the presence of disturbances in the range 1 to 100Hz, using 178 sensors and actuators positioned around the ring. This report describes the design of controller dynamics for this system.

2 System Model

Let $\mathbf{P}$(s) denote the transfer function between $\mathbf{U}(s) \in \mathbb{R}^N$, the inputs to the N actuators, and $\mathbf{Y}(s) \in \mathbb{R}^M$, the signals measured at the M sensors, such that

$$\mathbf{Y}(s) = \mathbf{P}(s)\mathbf{U}(s) \tag{1}$$

where $\mathbf{P}$(s) is assumed to take the form

$$\mathbf{P}(s) = p(s)\mathbf{B} \tag{2}$$

with $\mathbf{B} \in \mathbb{R}^{m\times n}$ being the steady state (dc) response of the actuators and $p(s)$ the scalar dynamics, which are taken to be the same for each actuator. The dynamics are modelled as a first order response plus delay and take the form

$$p(s) = \mathrm{e}^{-s\tau_d}\frac{a}{s+a} \tag{3}$$

where τ_d is the delay in the system and a is the bandwidth of the actuator response (in rad.s^{-1}).

For $M \geq N$, the singular value decomposition of $\mathbf{B}$ takes the form

$$\mathbf{B} = \mathbf{U}\begin{bmatrix}\mathbf{\Sigma}\\ \mathbf{0}\end{bmatrix}\mathbf{V}^{\mathrm{T}} \tag{4}$$

where $\mathbf{U} \in \mathbb{R}^{M\times M}$ and $\mathbf{V} \in \mathbb{R}^{N\times N}$ are respectively, the left and right singular vectors and $\mathbf{\Sigma} \in \mathbb{R}^{N\times N}$ is a diagonal matrix containing the singular values, $\sigma_1 \geq \sigma_2 \geq \cdots \geq \sigma_N$. By partitioning $\mathbf{U}$ so that

$$\mathbf{U} = [\mathbf{U}_1 \quad \mathbf{U}_2] \tag{5}$$

where $\mathbf{U}_1 \in \mathbb{R}^{M\times N}$ and $\mathbf{U}_2 \in \mathbb{R}^{M\times(M-N)}$,

$$\mathbf{B} = \mathbf{U}_1\mathbf{\Sigma}\mathbf{V}^{\mathrm{T}} \tag{6}$$

then (1) can be written as

$$\mathbf{U}_1^{\mathrm{T}}\mathbf{Y}(s) = p(s)\mathbf{\Sigma}\mathbf{V}^{\mathrm{T}}\mathbf{U}(s) \tag{7}$$

Defining $\overline{\mathbf{Y}}(s) = \mathbf{U}_1^{\mathrm{T}}\mathbf{Y}(s)$ and $\overline{\mathbf{U}}(s) = \mathbf{V}^{\mathrm{T}}\mathbf{Y}(s)$, projects the response into "modal space" so that

$$\overline{Y}_n(s) = \mathrm{e}^{-s\tau_d}\frac{a}{s+a}\sigma_n\overline{U}_n(s) \tag{8}$$

where $\overline{Y}_n(s)$ and $\overline{U}_n(s)$ are the nth elements of $\overline{\mathbf{Y}}(s)$ and $\overline{\mathbf{U}}(s)$ respectively.

3 Discrete Time Form

In practice, the control system is implemented in "sample and hold" mode, where the sensor takes measurements $\mathbf{y}[k]$ at times $\{t = kT : k \in \mathbb{Z}^+\}$, with T being the sample interval so that $\mathbf{y}[k] = \mathbf{y}(kT)$, and the actuator inputs are held constant at $\mathbf{u}[k]$ over the time interval $t \in [kT, (k+1)T)$. For each mode

$$\overline{y}_n[k] = p(z^{-1})\sigma_n\overline{u}_n[k] \tag{9}$$

Parameter	Value
a	$2\pi \times 10^2$ rad.s^{-1}
τ_d	3.31×10^{-4} s
T	10^{-4} s

Table 1: Values of parameters used in design

where $p(z^{-1})$ is discrete time transfer function associated with continuous transfer function (3) is (see Appendix A)

$$p(z^{-1}) = z^{-d}\frac{b_0 + b_1 z^{-1}}{1 - a_1 z^{-1}} \tag{10}$$

where d is the smallest integer satisfying $dT > \tau_d$ and

$$a_1 = \mathrm{e}^{-aT} \tag{11}$$

$$b_0 = 1 - \mathrm{e}^{-a(T-\tau')} \tag{12}$$

$$b_1 = \mathrm{e}^{-a(T-\tau')} - \mathrm{e}^{-aT} \tag{13}$$

with

$$\tau' = \tau_d - (d-1)T \tag{14}$$

The parameters associated with the beam stabilisation system are listed in Table 1 and the discrete time transfer function is

$$p(z^{-1}) = z^{-4}\frac{0.041 + 0.019 z^{-1}}{1 - 0.939 z^{-1}} \tag{15}$$

This transfer function has a minimum phase response because the zero occurs at $z = -0.46$, which is inside the unit circle. The step response and the frequency response for both continuous and discrete transfer functions are given in Figures 1 and 2.

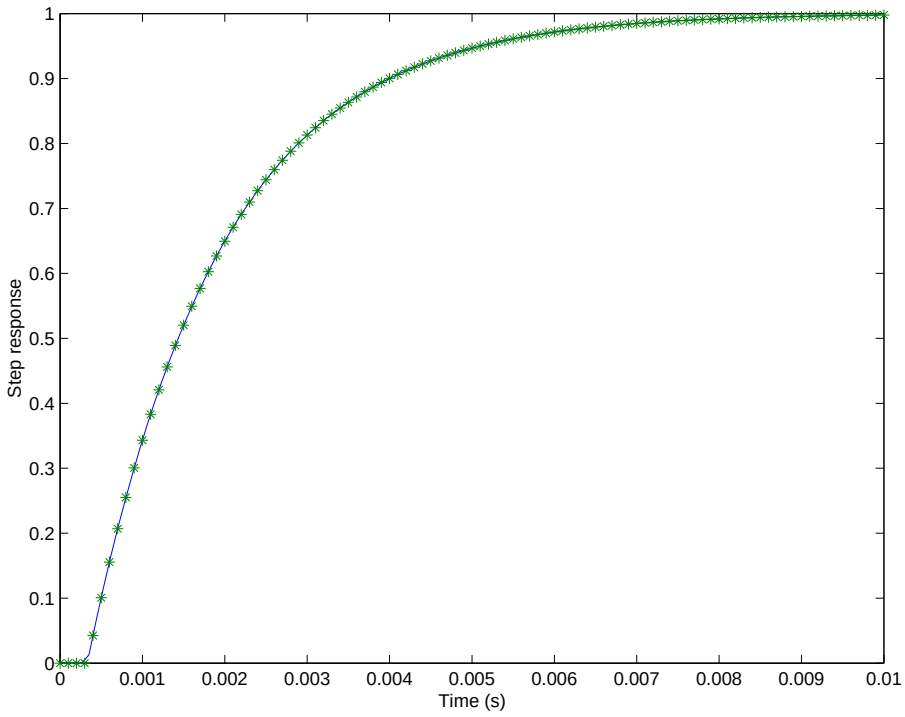


Figure 1: Plot of open loop step response for both continuous (blue solid line) and discrete sample and hold (green asterisks) transfer functions

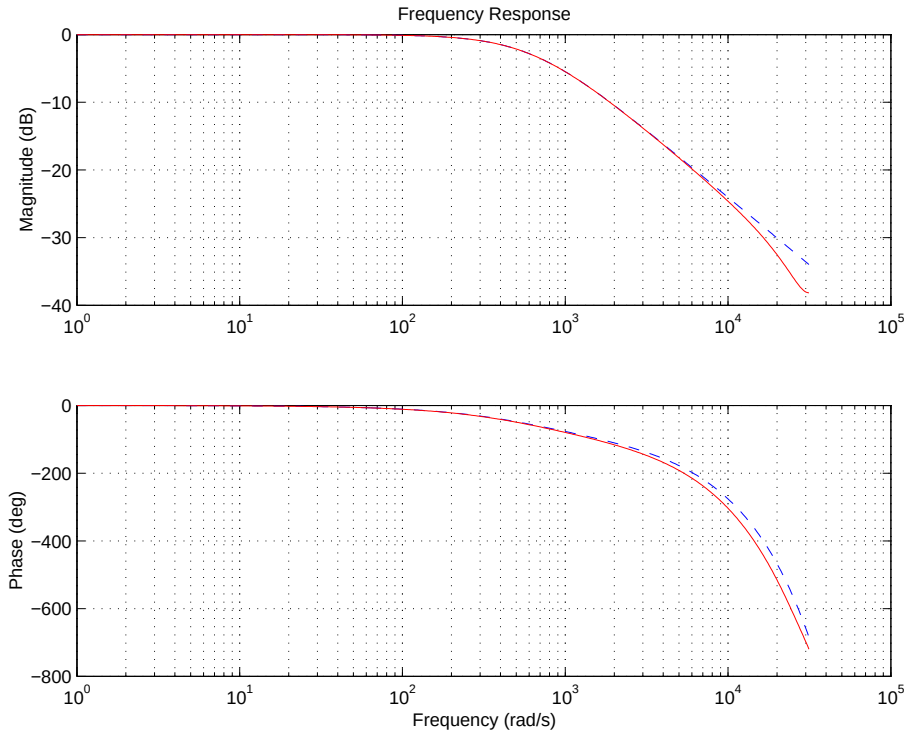


Figure 2: Plot of open loop frequency response for both continuous (blue dashed line) and discrete sample and hold (red solid line) transfer functions. The Nyquist sampling frequency is $\pi \times 10^4$ rad.s^{-1}

4 Design of an IMC Controller

The structure of an Internal Model Control (IMC) system is shown in Figure 3, where $q_n(z^{-1})$ is

$$q_n(z^{-1}) = \frac{(1-\lambda_n)}{1-\lambda_n z^{-1}} \frac{1-a_1 z^{-1}}{b_0 + b_1 z^{-1}} \tag{16}$$

where $\lambda_n = \mathrm{e}^{-\zeta_n T}$ and ζ_n is a tuning parameter, which can be different for each mode. This transfer function has a pole at $z = -b_1/b_0$. Although this represents a stable pole, because the pole lies on the negative real axis, it causes an oscillation in the inputs applied to the actuators that has a frequency equal to half the sampling frequency. Given that there is some degree of uncertainty in the exact value of the time constant of the actuator, this may also lead to the control signal "ringing" due to the inexact cancellation of the pole with the corresponding zero in the transfer function of the process $p(z^{-1})$. In addition, it makes the system prone to instabilities caused by uncertainties in the response of the process at high frequencies. For this reason, it is better to use

$$q_n(z^{-1}) = \frac{(1-\lambda_n)}{1-\lambda_n z^{-1}} \frac{1-a_1 z^{-1}}{(b_0 + b_1)} \tag{17}$$

where the scaling factor $(b_0 + b_1)$ ensures that the steady state gain of the controller is correct.

If the block diagram is rearranged to the form in Figure 4, the controller becomes

$$\mathbf{C}(z^{-1}) = \mathbf{V}\mathrm{diag}\left\{\frac{1}{\sigma_n} c_n(z^{-1})\right\} \mathbf{U}_1^{\mathrm{T}} \tag{18}$$

where the controller dynamics for each mode are

$$\frac{1}{\sigma_n} c_n(z^{-1}) = \frac{\frac{1}{\sigma_n} q_n(z^{-1})}{1 - \sigma_n p(z^{-1}) \frac{1}{\sigma_n} q_n(z^{-1})} \tag{19}$$

$$= \frac{1}{\sigma_n} \frac{q_n(z^{-1})}{1 - p(z^{-1}) q_n(z^{-1})} \tag{20}$$

so that

$$c_n(z^{-1}) = \frac{q_n(z^{-1})}{1 - p(z^{-1})q_n(z^{-1})} \tag{21}$$

Substituting for $p(z^{-1})$ from (10) and for $q_n(z^{-1})$ from (17) gives

$$c_n(z^{-1}) = \frac{(1-\lambda_n)}{(b_0+b_1)} \frac{1 - a_1 z^{-1}}{1 - \lambda_n z^{-1} - z^{-d}(1-\lambda_n)\beta(z^{-1})} \tag{22}$$

where

$$\beta(z^{-1}) = \beta_0 + \beta_1 z^{-1} = \frac{b_0 + b_1 z^{-1}}{b_0 + b_1} \tag{23}$$

Because $\beta_0 + \beta_1 = 1$, the second term in the denominator of (22) can be factored as

$$\begin{aligned} &1 - \lambda_n z^{-1} - z^{-d}(1-\lambda_n)\beta(z^{-1}) = \\ &\quad (1 - z^{-1})[1 + (1-\lambda_n)z^{-1} + (1-\lambda_n)z^{-2} + \cdots + (1-\lambda_n)z^{-(d-2)} + \beta_1(1-\lambda_n)z^{-(d-1)}] \end{aligned} \tag{24}$$

and the presence of the $(1 - z^{-1})$ term ensures that the controller includes integral action. In the process control literature, this controller is sometimes referred to as a Dahlin controller or a lambda controller (because the controller is tuned by adjusting λ_n).

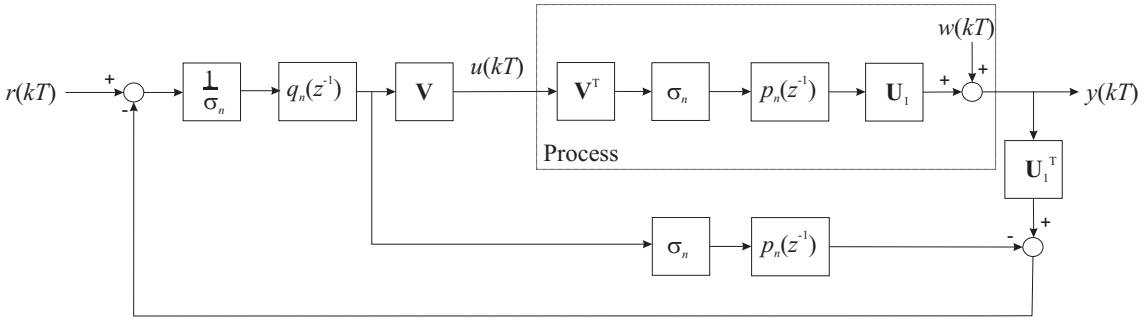


Figure 3: Structure of IMC controller

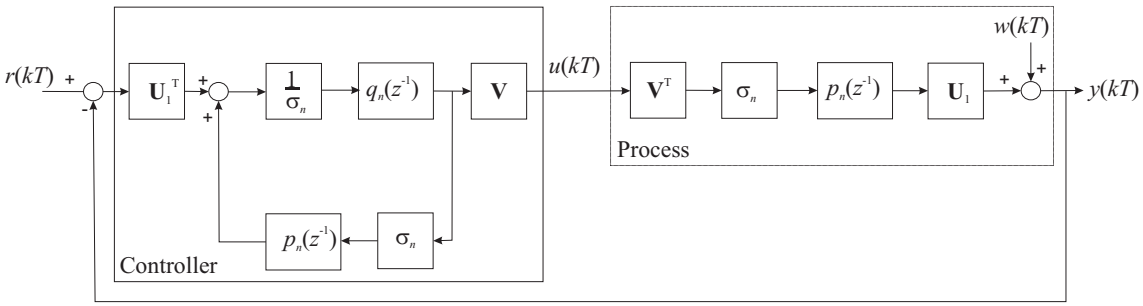


Figure 4: Alternative structure of IMC controller

5 Implementing the Controller

The controller shown in Figure 4 takes the form

$$\mathbf{C}(z^{-1}) = \mathbf{V}\text{diag}\left\{\frac{1}{\sigma_n} c_n(z^{-1})\right\}\mathbf{U}_1^{\mathrm{T}} \tag{25}$$

$$= \mathbf{V}\text{diag}\left\{\frac{1}{\sigma_n}\frac{(1-\lambda_n)}{(b_0+b_1)}\frac{1 - a_1 z^{-1}}{1 - \lambda_n z^{-1} - z^{-d}(1-\lambda_n)(\beta_0 + \beta_1 z^{-1})}\right\}\mathbf{U}_1^{\mathrm{T}} \tag{26}$$

The problem with this structure is that the calculation of the actuator inputs $\mathbf{u}[k]$ requires a multiplication by $\mathbf{U}_1^{\mathrm{T}}$ to convert the error into mode space. The controller dynamics are applied to these values and the result is then multiplied by $\mathbf{V}$ to convert from mode space to input space. Given that $\mathbf{B}$ has dimensions 178×178, the two matrix multiplications require a significant amount of computation. The controller is designed by choosing a separate ζ_n (and hence λ_n) for each mode and as a result, each mode has its own dynamics. An alternative approach is to use a common value of λ for all modes and to adjust the bandwidth of each mode by applying a different gain d_n to each mode, as in Figure 8. In this case, the control dynamics for each mode become

$$c_n(z^{-1}) = \frac{d_n}{\sigma_n} \frac{q(z^{-1})}{1 - p(z^{-1})q(z^{-1})} \tag{27}$$

$$= \frac{d_n}{\sigma_n} \frac{(1-\lambda_n)}{(b_0+b_1)} \frac{1 - a_1 z^{-1}}{1 - \lambda_n z^{-1} - z^{-d}(1-\lambda_n)(\beta_0 + \beta_1 z^{-1})} \tag{28}$$

where λ is the same for all modes. Since the denominator polynomial is the same as in (24), the transfer function contains a root at $z = 1$ and the controller includes integral action.

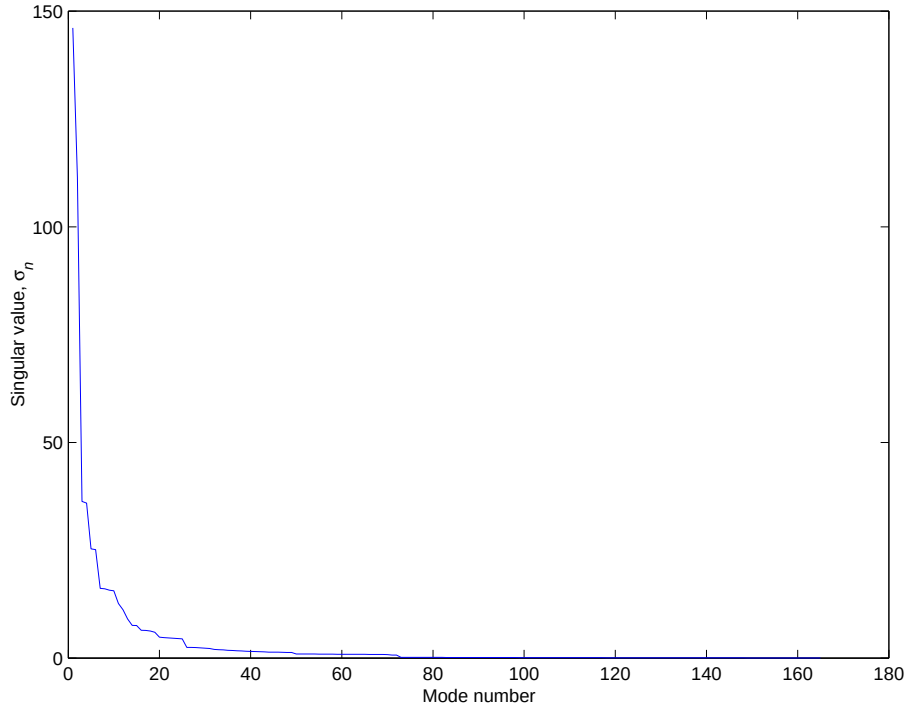


Figure 5: Singular values of steady state response matrix $\mathbf{B}$

The advantage of this structure is that it allows the controller to be implemented in the form in Figure 9, so that

$$\mathbf{C}(z^{-1}) = c(z^{-1})\mathbf{C} \tag{29}$$

where $\mathbf{C} \in \mathbb{R}^{N \times M}$ is

$$\mathbf{C} = \mathbf{V}\mathbf{D}\mathbf{\Sigma}^{-1}\mathbf{U}_1^{\mathrm{T}} \tag{30}$$

with

$$\mathbf{D} = \mathrm{diag}\,\{d_n\} \tag{31}$$

$$\mathbf{\Sigma} = \mathrm{diag}\,\{\sigma_n\} \tag{32}$$

and

$$c(z^{-1}) = \frac{(1-\lambda_n)}{(b_0+b_1)} \frac{1 - a_1 z^{-1}}{1 - \lambda_n z^{-1} - z^{-d}(1-\lambda_n)(\beta_0 + \beta_1 z^{-1})} \tag{33}$$

This structure means that only one matrix multiplication is required when generating the control actions. Multiplying the measurements from the sensors $\mathbf{y}[k]$ by $\mathbf{C}$ converts directly from output space to input

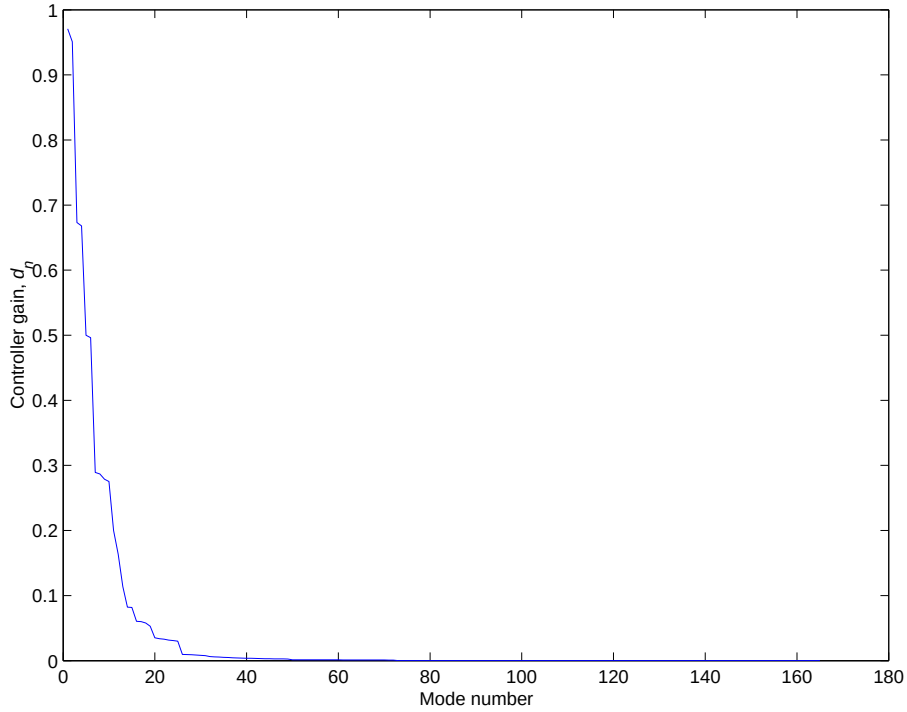


Figure 6: Values of controller gains, d_n, plotted against mode number for the singular values in Figure 5

space and the controller dynamics are then applied in the input space. Unlike the controller in (26), where different dynamics are applied to each mode through the choice of individual values of λ_n, in this controller each mode now has the same dynamics, but the response of each mode is detuned via the choice of d_n. One possible choice for the values of d_n is

$$d_n = \frac{\sigma_n^2}{\sigma_n^2 + \mu} \tag{34}$$

where μ is chosen so that $d_n \approx 1$ when $\sigma_n^2 >> \mu$ and $d_n \to 0$ when $\sigma_n^2 << \mu$. This ensures that the optimal control action is applied to the low order modes, but the control action is "switched off" for the high order modes, where the effect of modelling uncertainties is greatest and the control actions tend to be large. The singular values for $\mathbf{B}$ are shown in Figure 5 and for $\mu = {\sigma_5}^2$, the corresponding values of d_n are shown in Figure 6, which shows that the gain decreases monotonically to zero as $n \to N$, reducing the gain applied to the higher order modes. The values of d_n/σ_n for each mode are shown in Figure 7, which shows that there is a step change at $n = 71$ and for modes higher than this value, d_n/σ_n is effectively zero. To avoid the integral action in the controller dynamics integrating up these very small values, it is better to set $d_n/\sigma_n = 0$ for all $n > 71$.

The complementary sensitivity function, denoted by $\mathbf{T}(z^{-1})$, is the transfer function from the reference signal $\mathbf{r}[k]$ to the output $\mathbf{y}[k]$. If $\overline{\mathbf{r}}[k] = \mathbf{U}_1^{\mathrm{T}}\mathbf{r}[k]$, then for each mode, $t_n(z^{-1})$ is the closed loop transfer function from $\overline{r}_n[k]$ to $\overline{y}_n[k]$, which is given by

$$t_n(z^{-1}) = \frac{\sigma_n p(z^{-1}) \frac{d_n}{\sigma_n} c(z^{-1})}{1 + \sigma_n p(z^{-1}) \frac{d_n}{\sigma_n} c(z^{-1})} \tag{35}$$

$$= z^{-d} \frac{d_n(1-\lambda)(\beta_0 + \beta_1 z^{-1})}{1 - \lambda z^{-1} - z^{-d}(1-d_n)(1-\lambda)(\beta_0 + \beta_1 z^{-1})} \tag{36}$$

For the lower order modes, where $d_n \approx 1$, the complementary sensitivity function approaches

$$t_n(z^{-1}) = z^{-d} \frac{(1-\lambda)(\beta_0 + \beta_1 z^{-1})}{1 - \lambda z^{-1}} \tag{37}$$

so that the closed loop response to a step change in $\overline{r}_n[k]$ is a delayed first order response, where the time constant of the response is determined by λ. The zero of this transfer function occurs at $z = -\beta_1/\beta_0$

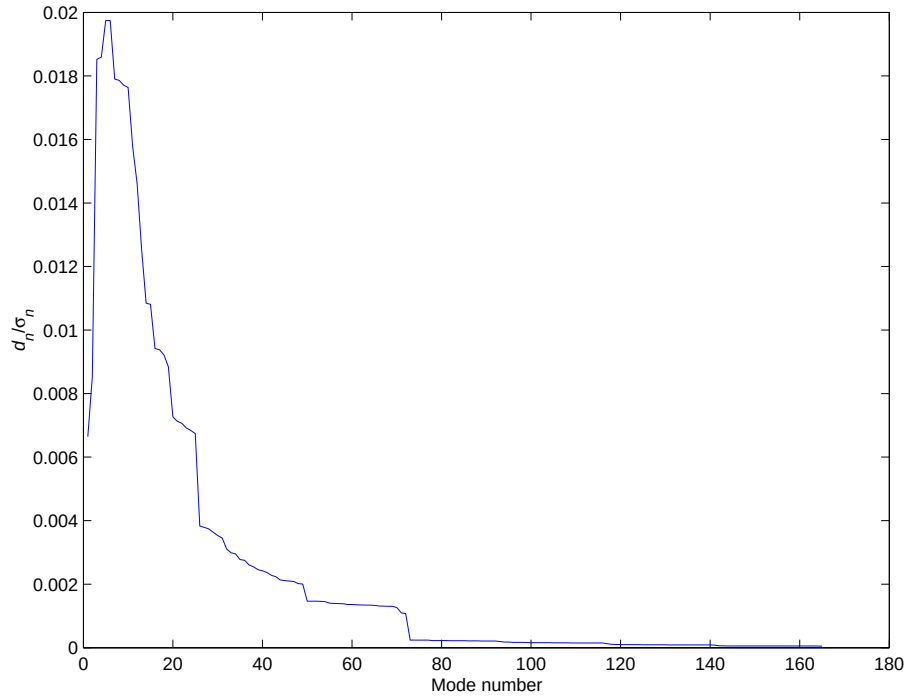


Figure 7: Values of d_n/σ_n plotted against mode number for the singular values in Figure 5

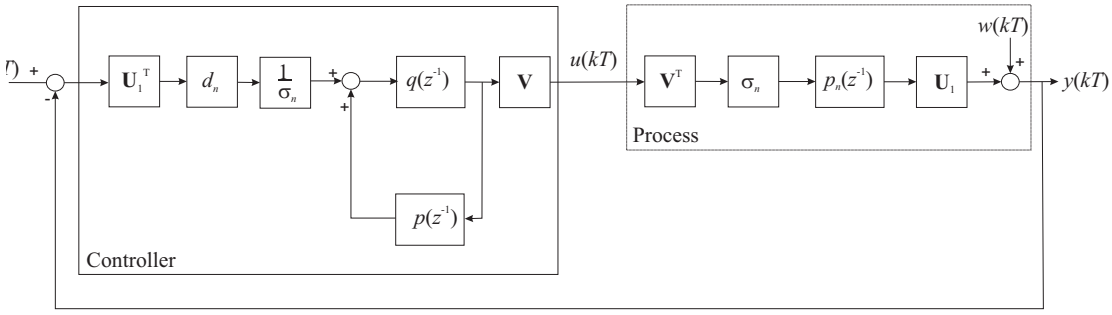


Figure 8: IMC controller including de-tuning gain d_n

which only has an effect at frequencies close to half the sampling frequency (*i.e.* the Nyquist frequency). Since the closed loop bandwidth will be much lower than the Nyquist frequency, the overall magnitude of the response will be unaffected by the presence of the zero.

The rule of thumb in the process industries is to choose ζ such that the time constant of the closed loop response is twice the time delay, so that $\zeta = 1/2\tau_d$, which gives $\lambda = \mathrm{e}^{-T/2\tau_d}$. For $\tau_d = 3.31 \times 10^{-4}$s, this corresponds to a closed loop bandwidth of $\zeta = 1.51 \times 10^3$rad.s^{-1} or 240Hz. However, for this application, this value of ζ is likely to be too conservative and in the designs presented below, the closed loop bandwidth is chosen to be $\zeta = 2\pi.400$rad.s^{-1}. Figure 10 shows the magnitude of the closed loop frequency responses for this value of λ with gains d_n corresponding to the first, fifth and tenth modes. For the first mode (where $d_1 = 0.97$, when $\mu = {\sigma_5}^2$), the closed loop bandwidth is almost equal to ζ, but for the higher order modes, where the controller gain is less than unity, ($d_5 = 0.50$ and $d_{10} = 0.27$ respectively), the closed loop bandwidth is reduced. For comparison, the closed loop frequency response of a PI controller of the form

$$c_{\mathrm{PI}}(z^{-1}) = K\left(1 + \frac{1}{T_i}\frac{T}{1 - z^{-1}}\right) \tag{38}$$

with $K = 2$ and $T_i = 1.4 \times 10^{-3}$s, is also shown and it can be seen that although the PI controller has a similar bandwidth, compared to the IMC controller, the amplification of disturbances occurs at lower

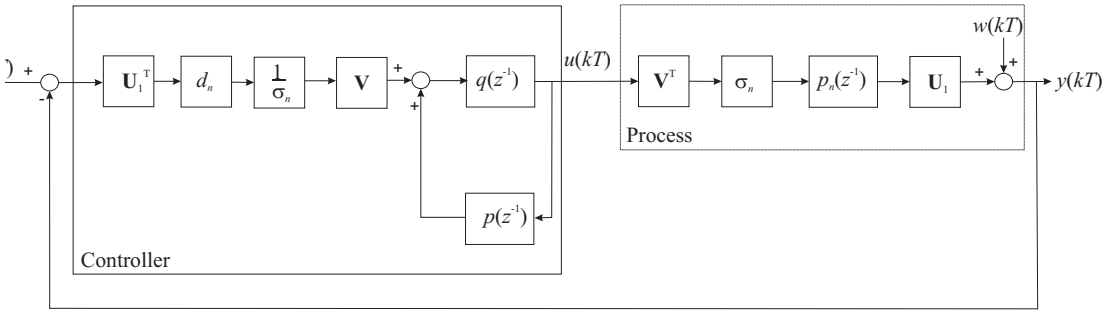


Figure 9: Alternative structure of IMC controller in Figure 8 that is suitable for implementation

frequencies.

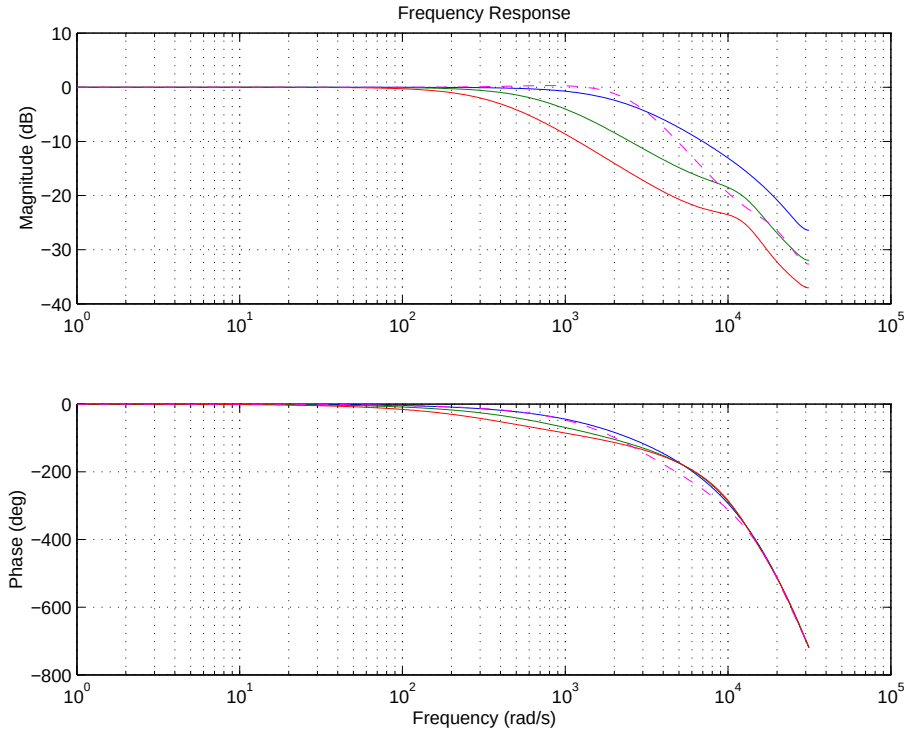


Figure 10: Frequency response of complementary sensitivity function $t_n(z^{-1})$ for three modes: $n = 1$ (blue solid line); $n = 5$ (green solid line) and $n = 10$ (red solid line), together with response of PI controller (magenta dashed line)

The sensitivity function, $\mathbf{S}(z^{-1})$, is the transfer function from the disturbance $\mathbf{w}[k]$ to the output $\mathbf{y}[k]$. If $\overline{\mathbf{w}}[k] = \mathbf{U}_1^{\mathrm{T}}\mathbf{w}[k]$, then for each mode, $s_n(z^{-1})$ is the transfer function from $\overline{w}_n[k]$, to the output, $\overline{y}_n[k]$, which is

$$s_n(z^{-1}) = 1 - t_n(z^{-1}) \tag{39}$$

$$= \frac{1 - \lambda_n z^{-1} - z^{-d}(1-\lambda)(\beta_0 + \beta_1 z^{-1})}{1 - \lambda z^{-1} - z^{-d}(1-d_n)(1-\lambda)(\beta_0 + \beta_1 z^{-1})} \tag{40}$$

The closed loop response to a step disturbance on a mode is shown in Figure 11 for the value of $\zeta = 2\pi.400\mathrm{rad.s}^{-1}$ for the first, fifth and tenth modes. For comparison, the response of the PI controller is also included and it can be seen that this response overshoots its steady state value.

Figure 12 shows the frequency responses of the sensitivity functions for the values of d_n used in Figure 10 as well as the PI controller, and it can be seen that decreasing d_n decreases the attenuation of the

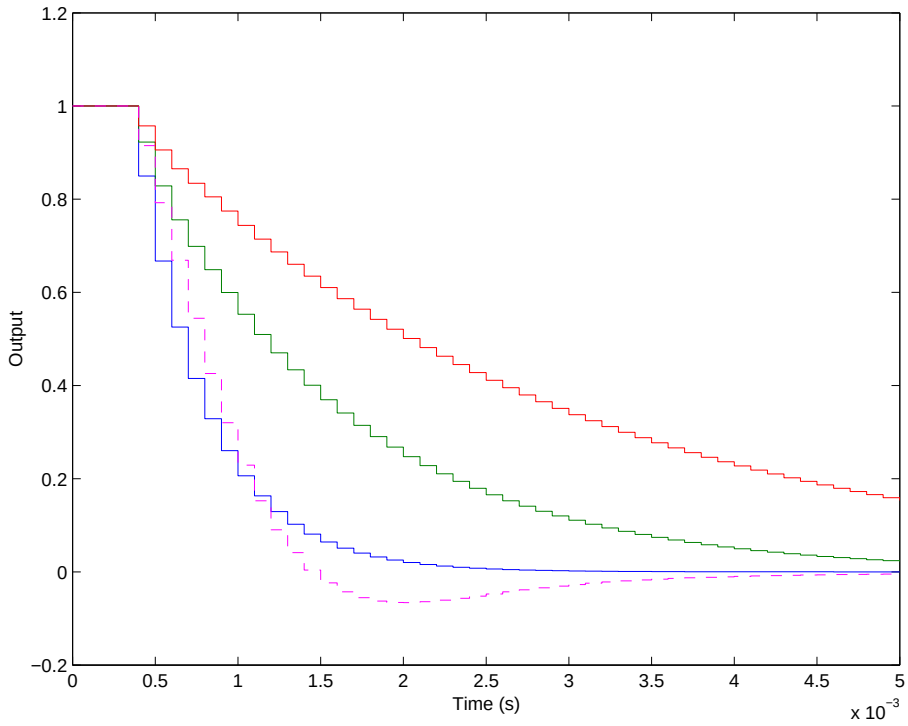


Figure 11: Closed loop response to step change in disturbance for three modes: $n = 1$ (blue solid line); $n = 5$ (green solid line) and $n = 10$ (red solid line), together with response of PI controller (magenta dashed line)

disturbance at low frequencies, although there is a corresponding reduction in the amplification at higher frequencies. Although the PI controller attenuates low frequency disturbances, compared to the IMC controllers, the amplification of the disturbances starts at a lower frequency.

Increasing d_n gives a faster step response and increases the attenuation of disturbances. However, to achieve this, larger control actions are required. The transfer function from $\overline{w}_n[k]$ to $\overline{u}_n[k]$ is given by

$$su_n(z^{-1}) = \frac{d_n}{\sigma_n} \frac{(1-\lambda)}{(b_0+b_1)} \frac{1-a_1 z^{-1}}{1-\lambda z^{-1} - z^{-d}(1-d_n)(1-\lambda)(\beta_0+\beta_1 z^{-1})} \tag{41}$$

This depends upon d_n/σ_n, which is plotted in Figure 7 for the case where $\mu = {\sigma_5}^2$. It can be seen that d_n/σ_n increases for the first five modes and then decreases for the higher order modes. The frequency response of this transfer function is plotted in Figure 13 for first, fifth and tenth modes, together with the response of the 5th mode when the PI controller is applied. The plot shows that the PI controller uses considerably larger control actions and as a result, is likely to be more sensitive to modelling errors unless the proportional gain is reduced for the higher order modes.

6 Design of the Controller

Figure 14 shows 10 seconds of the disturbance, $y_m[k]$, observed by the sensor corresponding to $m = 100$, when the beam positioning system is switched off and it can be seen that there is a significant disturbance affecting the system.[1] The mean deviation has been removed from the signal, so the variance of this disturbance is $E[y_m[k]^2] = 2.8 \times 10^7 \text{nm}^2$, which corresponds to a standard deviation of 5.3μm (although the standard deviation varies considerably between sensors, depending on their location around the ring). The frequency content of the disturbance is shown in Figure 15, which plots the magnitude of the

[1]The readings from sensors 23, 44 and 113 were ignored as they had unusually high standard deviations and/or high mean values. As a result, readings from only 165 sensors were used in the analysis.

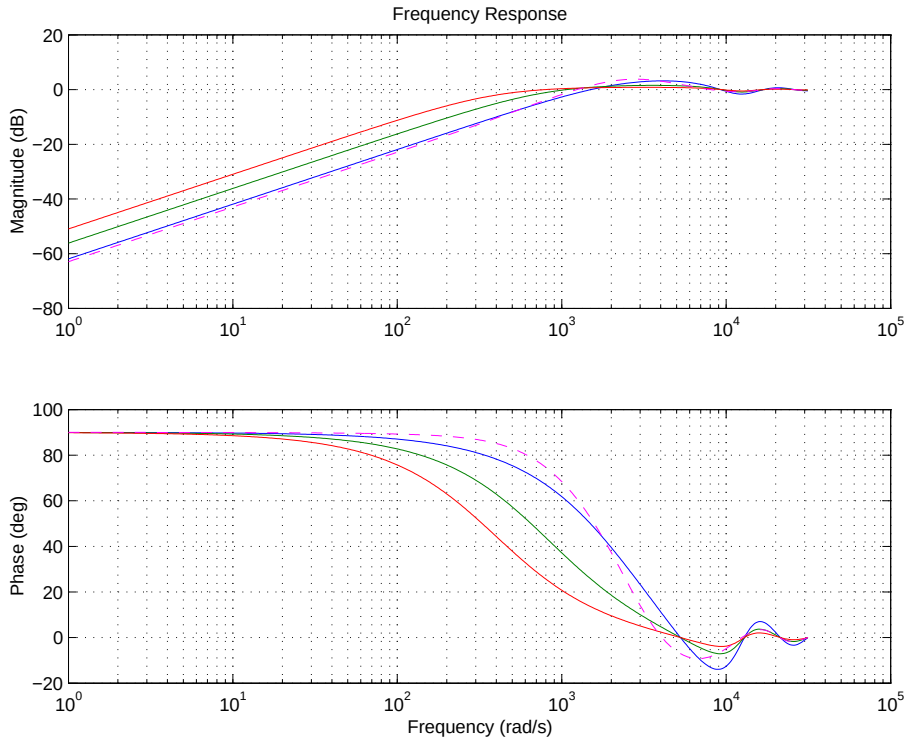


Figure 12: Frequency response of sensitivity function $S_n(z^{-1})$ for three modes: $n = 1$ (blue solid line); $n = 5$ (green solid line) and $n = 10$ (red solid line), together with response of PI controller (magenta dashed line)

discrete Fourier transform of the signal against frequency. It can be seen that the frequency distribution is concentrated between 15Hz and 30Hz, with a major peak at 25Hz, although there is also a component close to 50Hz. Although of smaller magnitude, there is also some variation at low frequencies (< 1Hz) and in practice, this is observed as a slow drift over time periods of the order of 10s.

Figure 16 shows a colour map of the average power (in dB) at each frequency within each of the modes and it can be seen that the bulk of the power is concentrated in the lower order modes (*i.e.* for $n < 10$), although the disturbances at 25Hz and 27Hz have a significant effect on all modes. The low frequency drift is also present in all modes. The aim of the control system is to reduce the effect of the disturbances on the beam, particularly for the low order modes in the frequency range 15Hz and 30Hz, while at the same time, attenuating low frequency disturbances (< 1Hz) in all modes. The control system needs to be robust to uncertainties in the model, which will have the biggest effect when controlling the higher order modes. The control design needs to balance these conflicting requirements and reduces to the choice of a suitable ζ which will provide sufficient bandwidth to attenuate the disturbances and a value of μ that will result in values of d_n that will focus the control effort on the lower order modes. However, the controller also needs to provide attenuation at low frequencies for all modes, in order to respond to the slow drift in the beam.

The expected value of the total power in the output is

$$E\|\mathbf{y}[k]\|_2^2 = \frac{1}{K}\sum_{k=0}^{K-1}\|\mathbf{y}[k]\|_2^2 \tag{42}$$

Since $\mathbf{U}$ is an orthogonal matrix, $\|\overline{\mathbf{y}}[k]\|_2 = \|\mathbf{U}_1\mathbf{y}[k]\|_2 = \|\mathbf{y}[k]\|_2$, so

$$E\|\mathbf{y}[k]\|_2^2 = \frac{1}{K}\sum_{k=0}^{K-1}\|\overline{\mathbf{y}}[k]\|_2^2 \tag{43}$$

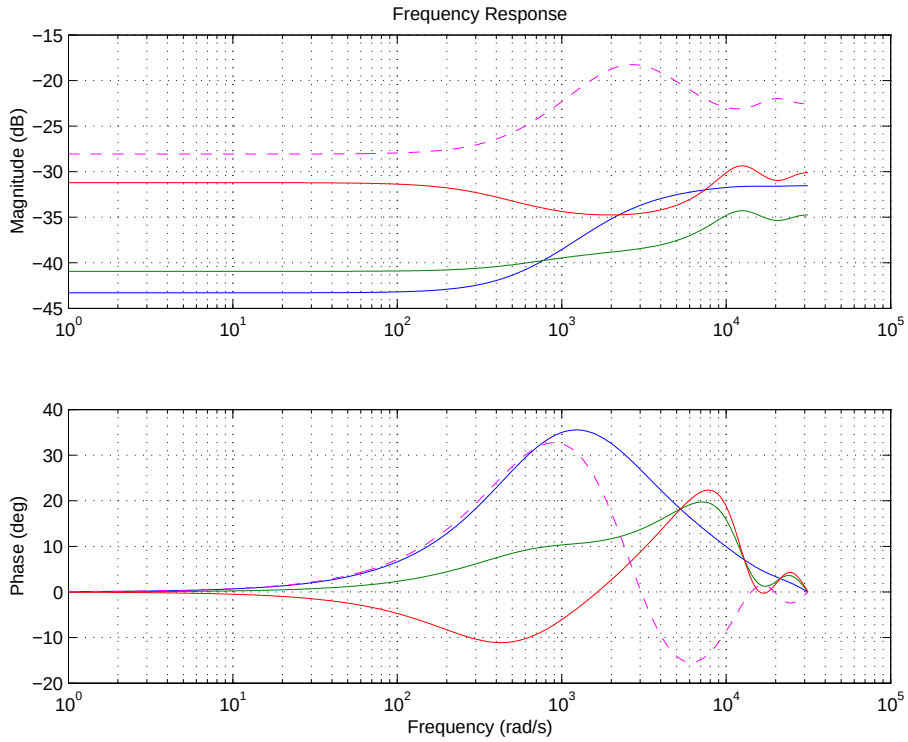


Figure 13: Frequency response of control sensitivity function $su_n(z^{-1})$ for three modes: $n = 1$ (blue solid line); $n = 5$ (green solid line) and $n = 10$ (red solid line), together with response of the 5th mode when the PI controller is applied (magenta dashed line)

Defining the discrete Fourier transform (DFT) of $\overline{\mathbf{y}}[k]$ as[2]

$$\overline{\mathbf{Y}}[p] = \sum_{k=0}^{K-1} \overline{\mathbf{y}}[k] \mathrm{e}^{-\mathrm{j}2\pi pk/K} \tag{44}$$

where $\{p = 0, 1, \ldots, K-1\}$, then

$$\sum_{k=0}^{K-1} \|\overline{\mathbf{y}}[k]\|_2^2 = \frac{1}{K} \sum_{p=0}^{K-1} \|\overline{\mathbf{Y}}[p]\|_2^2 \tag{45}$$

and

$$E\|\mathbf{y}[k]\|_2^2 = \frac{1}{K^2} \sum_{p=0}^{K-1} \|\overline{\mathbf{Y}}[p]\|_2^2 \tag{46}$$

Since

$$\|\overline{\mathbf{Y}}[p]\|_2^2 = \sum_{n=1}^{N} |\overline{Y}_n[p]|^2 \tag{47}$$

and $\overline{y}_n[k] = s_n(z^{-1})\overline{w}_n[k]$, then

$$\|\overline{\mathbf{Y}}[p]\|_2^2 = \sum_{n=1}^{N} |S_n[p]|^2 |\overline{W}_n[p]|^2 \tag{48}$$

where $S_n[p]$ is the frequency response of $s_n(z^{-1})$

$$S_n[p] = s_n(\mathrm{e}^{-\mathrm{j}2\pi pk/K}) \tag{49}$$

[2]This definition of the DFT follow [1] by including the factor $1/N$ in the inverse DFT, rather than the more standard approach in *e.g.* [2], which is more consistent with the continuous time Fourier transform in that it defines $\overline{\mathbf{Y}}[p] = \frac{1}{K}\sum_{k=0}^{K-1} \overline{\mathbf{y}}[k]\mathrm{e}^{-\mathrm{j}2\pi pk/K}$. If required, the analysis presented here can easily be modified to use this definition.

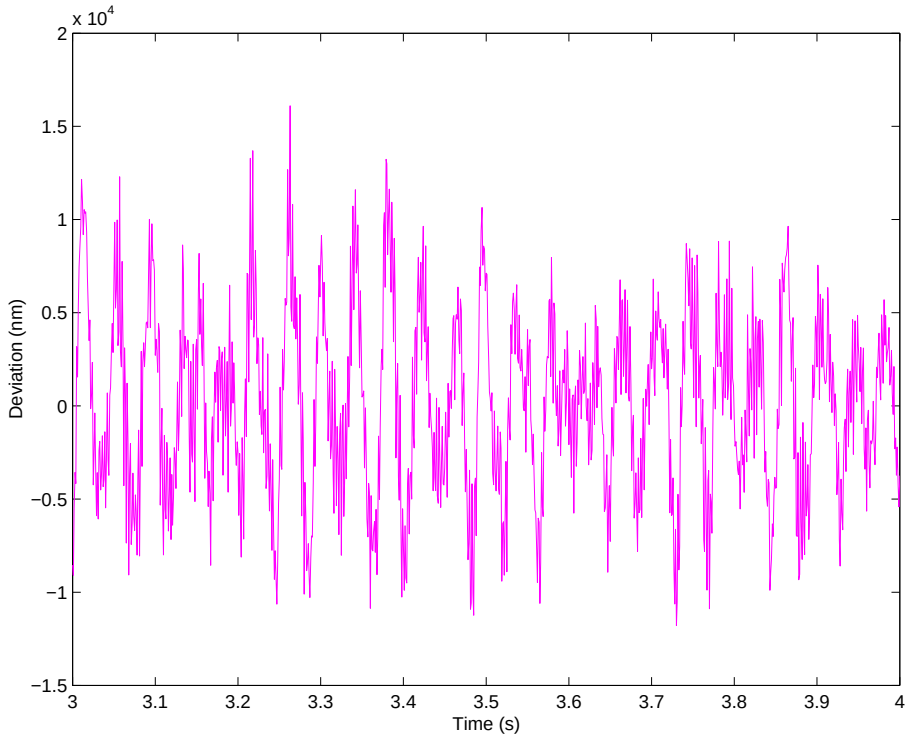


Figure 14: Variation in nm over a 1s section of measurements taken by the 100th sensor

Combining (49) and (46) gives

$$E\|\mathbf{y}[k]\|_2^2 = \frac{1}{K^2}\sum_{p=0}^{K-1}\sum_{n=1}^{N}|S_n[p]|^2|\overline{W}_n[p]|^2 \tag{50}$$

which implies that given $\overline{W}_n[p]$, the frequency spectrum of each mode of the underlying disturbance, $S_n[p]$ (and hence $s_n(z^{-1})$) can be designed on a "mode-by-mode" basis in order to achieve a specification on the expected total power observed across all sensors.

Using a closed loop bandwidth of $\zeta = 2\pi.400\text{rad.s}^{-1}$ and $\mu = {\sigma_5}^2$, the controller gain, d_n, associated with each mode is plotted in Figure 6, which shows that the controller gain reduces to 0.5 for the 5th mode and is small for modes higher than $n = 40$. As a result, the control action is concentrated in the lower order modes and Figure 17 shows the attenuation of disturbances at 25Hz at each mode. The attenuation at this frequency is restricted to the first 10 modes and there is a (very small) amplification of modes 20 to 25. Figure 18 shows that there is still significant attenuation at 0.1Hz up to about mode 70, even though the controller gain is very small for $n > 40$, indicating that the underlying slow drift will be regulated.

When the controller is applied to the underlying disturbance, the attenuation of the signal observed on the 100th sensor is shown in Figure 19 and it can be seen that there is a significant reduction in amplitude of the variation. Although this result could have been obtained by taking the DFT of the measurement signal and then multiplying by $S_n[p]$, it is easier to generate the plot by using the `lsim` function in Matlab to generate $\overline{y}_n[k]$ by filtering each mode of the disturbance $\overline{w}_n[k]$ through the corresponding sensitivity transfer function $s_n(z^{-1})$ and then recombining the modes using $\mathbf{y}[k] = \mathbf{U}_1^{\mathrm{T}}\overline{\mathbf{y}}[k]$. Figure 20 shows the cumulative frequency content of both the controlled and uncontrolled output and it can be seen that the power of the controlled signal is reduced by a factor of 4.4, corresponding to a reduction in standard deviation of about 46%. The standard deviation of the uncontrolled disturbance varies considerably between sensors and 21 shows the deviation of both the uncontrolled and the controlled output for all sensors. It can be seen that there is a significant reduction in the deviation on all sensors and as shown in Figure 22, the average reduction is around 46%.

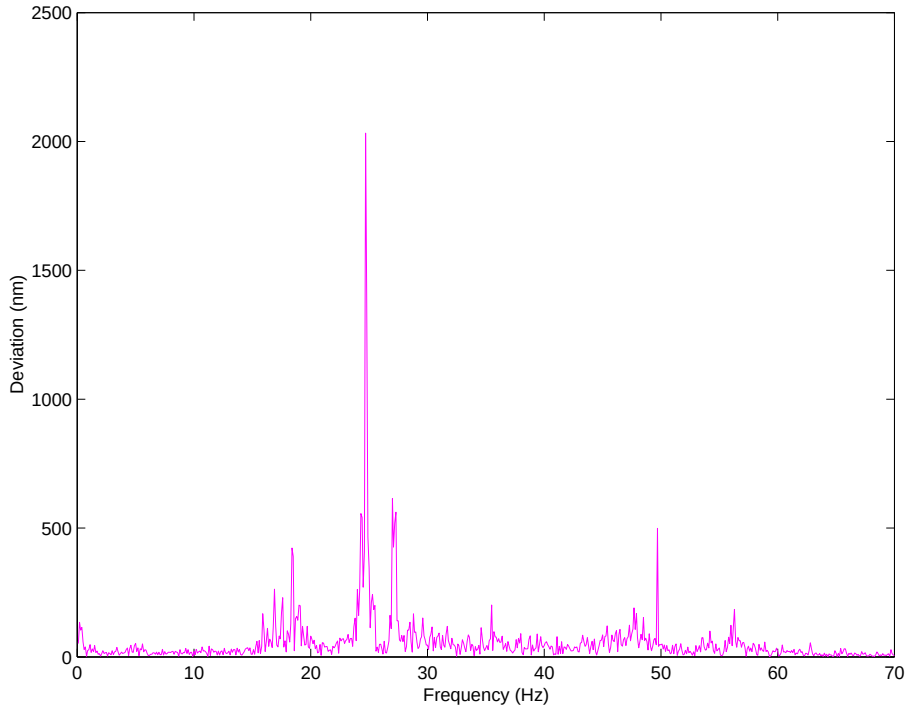


Figure 15: Magnitude of frequency response of 10s of variation observed at 100th sensor plotted against frequency in Hz

7 Robustness

7.1 Gain and Phase Margins

Robustness to uncertainties in the gain and phase of the dynamics can be expressed in terms of the gain and phase margins, which are obtained from the Nyquist plot of the open loop transfer function

$$\ell_n(z^{-1}) = \sigma_n p(z^{-1}) \frac{d_n}{\sigma_n} c_n(z^{-1}) \tag{51}$$

$$= z^{-d} \frac{d_n(1-\lambda)(\beta_0+\beta_1 z^{-1})}{1-\lambda z^{-1} - z^{-d}(1-d_n)(1-\lambda_n)(\beta_0+\beta_1 z^{-1})} \tag{52}$$

The Nyquist plot is the locus of $\ell_n(z^{-1})$ for $z = \mathrm{e}^{\mathrm{j}\omega T}$ as ω is varied over the interval $\omega \in [0, \pi/2T]$ and the plots for the three values of d_1, d_5 and d_{10} are shown in Figure 23. The corresponding gain and phase margins for these modes are given in Table 2. The table shows that decreasing d_n, increases both the gain and phase margins, making the closed loop system more robust to both errors in the steady state gain of the dynamics and/or σ_n, and the phase of dynamics. As a result, the robust stability of the overall system will be determined by the margins associated with the first mode. The phase margin is important in this system as it gives a measure of the allowable error in the delay τ_d that can be tolerated while the closed loop system remains stable. Since ω_{pc}, the frequency at which $|\ell_n(\mathrm{e}^{-\mathrm{j}\omega T})| = 1$, is 1.26×10^3 rad.s^{-1}, a small error in τ_d can make a large change in argument of $\ell_n(\mathrm{e}^{-\mathrm{j}\omega T})$ at this frequency. The system can tolerate an error of $\Delta\tau_d$ that satisfies

$$\Delta\tau_d < \frac{69.2}{180} \frac{\pi}{1.26 \times 10^3} \tag{53}$$

$$< 0.96\text{ms} \tag{54}$$

The last row of the table gives the corresponding gain and phase margins for the PI controller, which shows that while the gain margin is similar to the IMC design, the phase margin is considerably less.

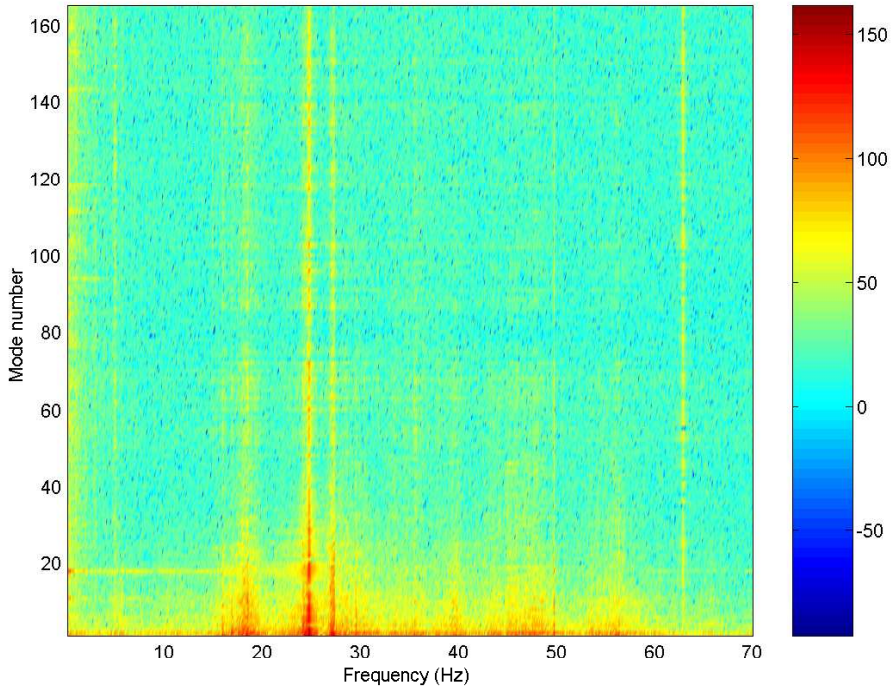


Figure 16: Colormap of average power in dB for each mode against frequency in Hz

n	d_n	Gain Margin	ω_{gc} rad.s^{-1}	Phase Margin deg	ω_{pc} rad.s^{-1}	γ	ω_γ rad.s^{-1}
1	0.97	3.47	5.28×10^3	69.2	1.26×10^3	0.69	4.11×10^3
5	0.50	6.73	5.28×10^3	79.4	0.64×10^3	0.84	3.56×10^3
10	0.28	12.23	5.28×10^3	84.2	0.35×10^3	0.91	3.11×10^3
		3.38	4.07×10^3	59.3	1.25×10^3	0.64	2.81×10^3

Table 2: Gain and phase margins and γ values for different values for $n = 1$, $n = 5$ and $n = 10$. The fourth row gives the corresponding values for the PI controller

7.2 Errors in Steady State Response

The previous section has considered robustness to errors in the scalar dynamics and/or simple scaling of the singular values σ_n. A second major source of uncertainty in the model is associated with the steady state response of the actuators $\mathbf{B}$. If the actual steady state response is denoted by $\tilde{\mathbf{B}}$, then this can be considered as a perturbation from the nominal steady state response $\mathbf{B}$, so that

$$\tilde{\mathbf{B}} = \mathbf{B} + \mathbf{E} \tag{55}$$

where $\mathbf{E}$ is the model uncertainty. If $\mathbf{U}$ and $\mathbf{V}$ contain the left and right singular vectors of the nominal response matrix $\mathbf{B}$, then

$$\tilde{\mathbf{B}} = \mathbf{U} \begin{bmatrix} \mathbf{\Sigma} \\ \mathbf{0} \end{bmatrix} \mathbf{V}^{\mathrm{T}} + \mathbf{U}\mathbf{\Delta}\mathbf{V}^{\mathrm{T}} \tag{56}$$

where $\mathbf{E} = \mathbf{U}\mathbf{\Delta}\mathbf{V}^{\mathrm{T}}$, which unlike the SVD of $\mathbf{B}$, need not consist of an upper block containing a diagonal matrix and a zero lower block. As a result, the effect of this perturbation can introduce cross-coupling between the responses of the individual modes.

The analysis of Appendix B shows that the system will remain stable in the presence of uncertainties in $\mathbf{B}$ provided that the minimum distance between the $-1 + \mathrm{j}0$ point and the Nyquist plot associated with

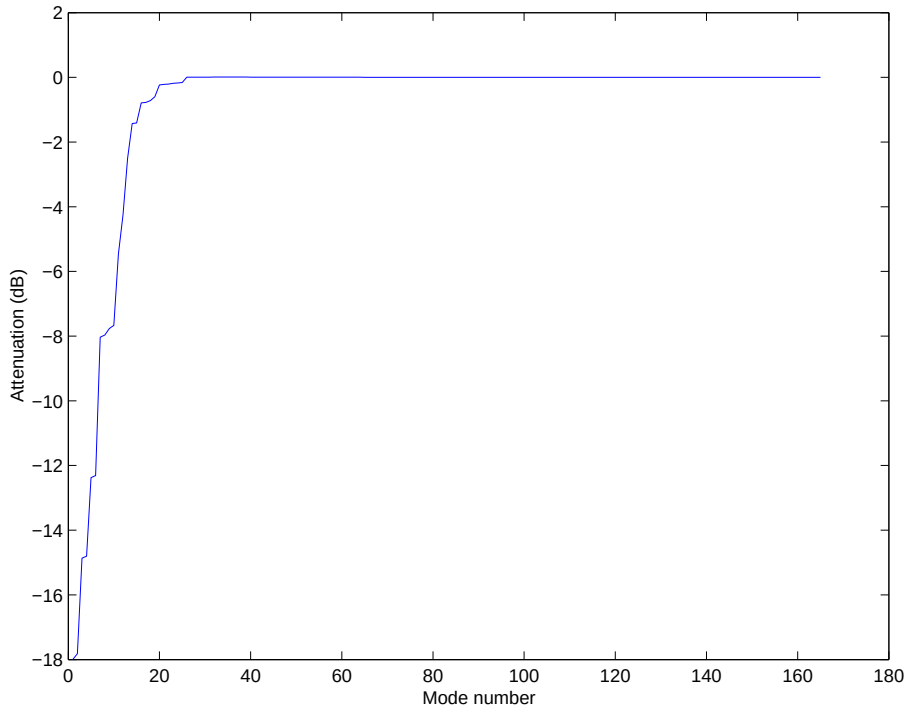


Figure 17: Plot of attenuation (in dB) of disturbance at 25Hz for each mode

the first mode exceeds $\|\mathbf{\Delta}\Sigma^{-1}\mathbf{D}\|_2$. If this minimum distance is denoted by γ, so that

$$\gamma = \min_{\omega} \left\{ \left| 1 + \frac{\sigma_1}{{\sigma_1}^2 + \mu} p(\mathrm{e}^{-\mathrm{j}\omega T}) c(\mathrm{e}^{-\mathrm{j}\omega T}) \right| \right\} \tag{57}$$

then to maintain stability in the presence of the perturbation $\mathbf{E}$, it is necessary to ensure that

$$\gamma > \|\mathbf{\Delta}\Sigma^{-1}\mathbf{D}\|_2 \tag{58}$$

$$> \|\mathbf{\Delta}\|_2 \|\Sigma^{-1}\mathbf{D}\|_2 \tag{59}$$

Since $\|\mathbf{\Delta}\|_2 = \|\mathbf{U}\mathbf{\Delta}\mathbf{V}^{\mathrm{T}}\|_2 = \|\mathbf{E}\|_2$, this reduces to

$$\|\mathbf{E}\|_2 < \frac{\gamma}{\|\Sigma^{-1}\mathbf{D}\|_2} \tag{60}$$

where

$$\|\Sigma^{-1}\mathbf{D}\|_2 = \max\left\{\frac{d_n}{\sigma_n}\right\} = \max\left\{\frac{\sigma_n}{{\sigma_n}^2 + \mu}\right\} \tag{61}$$

for the choice of d_n in (34). It can be shown that

$$\|\Sigma^{-1}\mathbf{D}\|_2 = \frac{1}{2\sqrt{\mu}} \tag{62}$$

so that the condition for robust stability in (60) becomes

$$\|\mathbf{E}\|_2 < 2\sqrt{\mu}\gamma \tag{63}$$

Increasing μ has the effect of decreasing $\|\Sigma^{-1}\mathbf{D}\|_2$, which in turn, increases the norm of the allowable uncertainty, $\mathbf{E}$. It also has the effect of increasing γ, giving a larger stability margin. Table 2 gives the value of γ obtained from the Nyquist plots in Figure 23 and for $\mu = {\sigma_5}^2$, this leads to the requirement that $\|\mathbf{E}\|_2 < 35.0$. Given that $\|\mathbf{B}\|_2 = 146.1$, which corresponds to a 24.0% allowable error in the norm of the steady state response.

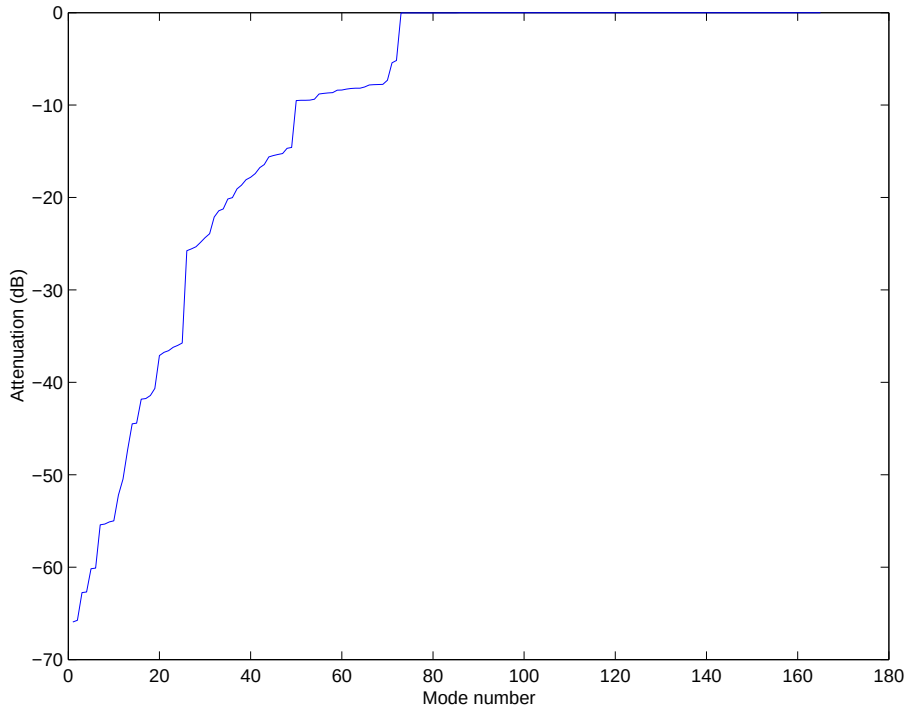


Figure 18: Plot of attenuation (in dB) of disturbance at 0.1Hz for each mode

Appendix A. Derivation of Discrete Time Transfer Function

If

$$Y(s) = p(s)U(s) \tag{64}$$

where

$$p(s) = \mathrm{e}^{-s\tau'}\frac{a}{s+a} \tag{65}$$

then

$$\frac{dy}{dt} + ay(t) = au(t-\tau') \tag{66}$$

The continuous output, $y(t)$, is sampled at times $\{t = kT : k \in \mathbb{Z}^+\}$ to give a sequence of samples $y[k]$. The inputs remain fixed over the period between samples, so that $u(t) = u[k]$ for $t \in [kT, (k+1)T)$. The aim is to express $y[k]$ in terms of past outputs $\{y[k-1], y[k-2], \dots\}$, and current and past inputs $\{u[k], u[k-1], u[k-2], \dots\}$. Initially, it will be assumed that $\tau' < T$. The analysis will then be extended to handle the case where the time delay exceeds the sample period.

From (66),

$$\mathrm{e}^{at}\frac{dy}{dt} + a\mathrm{e}^{at}y(t) = a\mathrm{e}^{at}u(t-\tau') \tag{67}$$

so that

$$\frac{d}{dt}\left[\mathrm{e}^{at}y(t)\right] = a\mathrm{e}^{at}u(t-\tau') \tag{68}$$

Integrating over the interval $t \in [(k-1)T, kT]$ gives

$$\int_{t=(k-1)T}^{t=kT}\frac{d}{dt}\left[\mathrm{e}^{at}y(t)\right]dt = a\int_{t=(k-1)T}^{t=kT}\mathrm{e}^{at}u(t-\tau')dt \tag{69}$$

$$\mathrm{e}^{akT}y(kT) - \mathrm{e}^{a(k-1)T}y[(k-1)T] = a\int_{t=(k-1)T}^{t=kT}\mathrm{e}^{at}u(t-\tau')dt \tag{70}$$

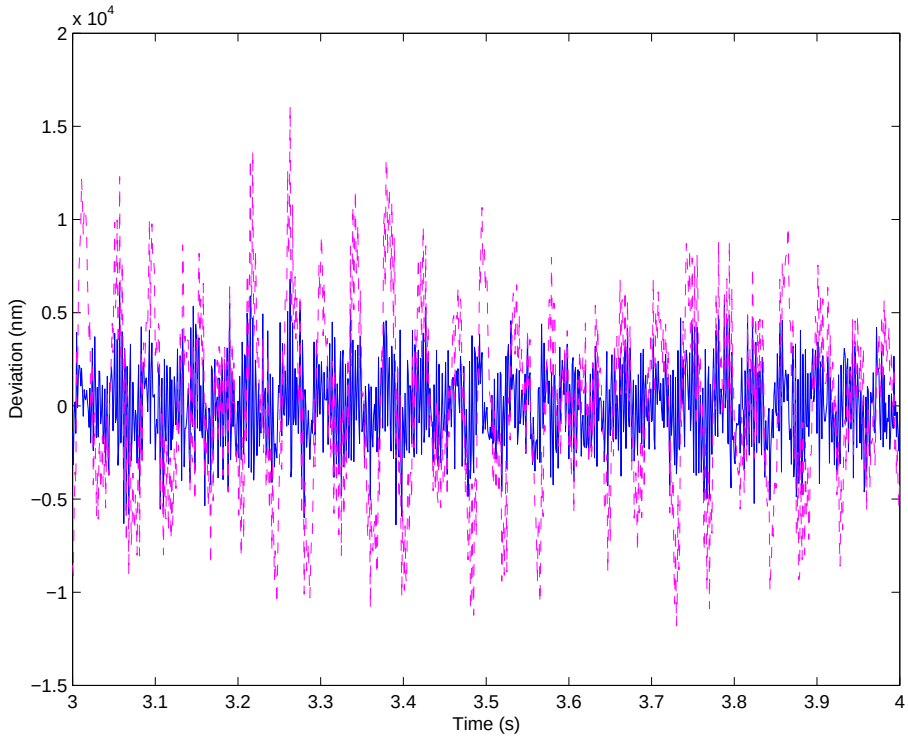


Figure 19: Controlled (blue) and uncontrolled (magenta dashed line) variations in nm over a 1s section of measurements taken by the 100th sensor

Writing $y[k] = y(kT)$ leads to

$$y[k] = \mathrm{e}^{-aT} y[k-1] + a \int_{t=(k-1)T}^{t=kT} \mathrm{e}^{-a(kT-t)} u(t-\tau')dt \tag{71}$$

Substituting $t_1 = t - \tau'$ into the integral in (71)

$$y[k] = \mathrm{e}^{-aT} y[k-1] + a \int_{t_1=(k-1)T-\tau'}^{t_1=kT-\tau'} \mathrm{e}^{-a(kT-\tau'-t_1)} u(t_1)dt_1 \tag{72}$$

For the period $(k-1)T - \tau' \leq t_1 \leq (k-1)T$, the input is a constant value, $u(t_1) = u[k-2]$. Similarly for $(k-1)T \leq t_1 \leq kT - \tau'$, $u(t_1) = u[k-1]$, so that

$$\begin{aligned} y[k] &= \mathrm{e}^{-aT} y[k-1] + au[k-1] \int_{t_1=(k-1)T}^{t_1=kT-\tau'} \mathrm{e}^{-a(kT-\tau'-t_1)} dt_1 \\ &\qquad + au[k-2] \int_{t_1=(k-1)T-\tau'}^{t_1=(k-1)T} \mathrm{e}^{-a(kT-\tau'-t_1)} dt_1 \qquad (73) \\ &= \mathrm{e}^{-aT} y[k-1] + \left(1 - \mathrm{e}^{-a(T-\tau')}\right) u[k-1] + \left(\mathrm{e}^{-a(T-\tau')} - \mathrm{e}^{-aT}\right) u[k-2] \qquad (74) \end{aligned}$$

Using the backward shift operator, z^{-1}, where $z^{-1}y[k] = y[k-1]$, gives

$$y[k] = z^{-1} \frac{b_0 + b_1 z^{-1}}{1 - a_1 z^{-1}} u[k] \tag{75}$$

where b_0, b_1 and a_1 are given in (11) to (13).

For the case where the delay $\tau_d > T$, by writing $\tau' = \tau_d - (d-1)T$, this introduces an extra delay of $(d-1)T$, leading to the discrete time transfer function in (10).

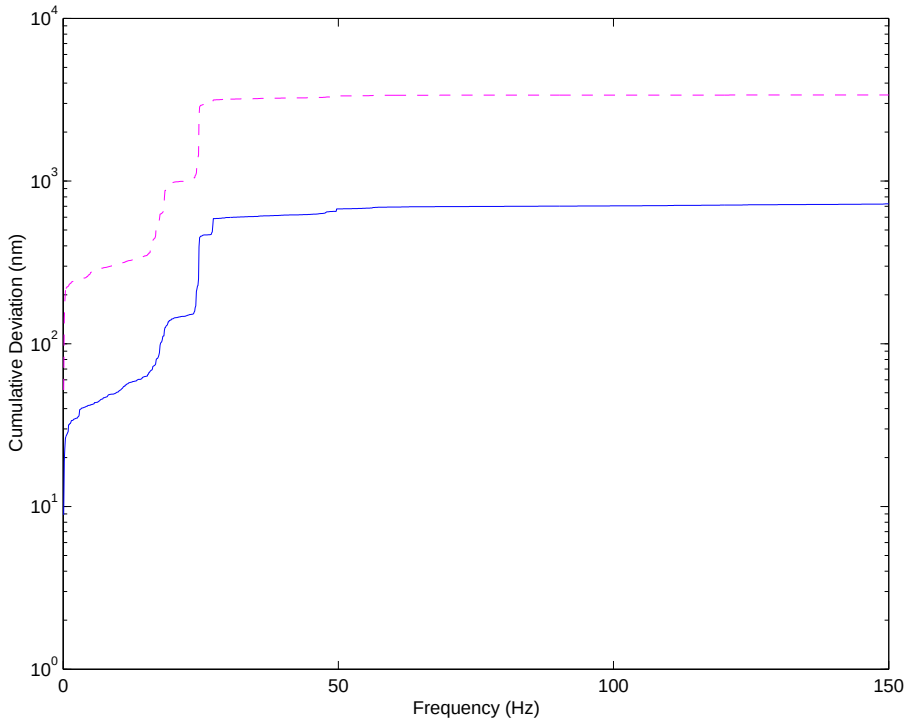


Figure 20: Cumulative magnitude of frequency response of 10s of controlled (blue line) and uncontrolled (magenta dashed line) variations observed at 100th sensor plotted against frequency in Hz

Appendix B. Derivation of Bound on Perturbation

Let the true steady state response matrix be defined as $\tilde{\mathbf{B}} = \mathbf{B} + \mathbf{E}$, where $\mathbf{E} \in \mathbb{R}^{m \times n}$ is an unknown perturbation from the nominal response matrix $\mathbf{B}$. The true plant response is therefore

$$\tilde{\mathbf{P}}(z^{-1}) = p(z^{-1})[\mathbf{B} + \mathbf{E}] \tag{76}$$

Using the SVD of the nominal response matrix

$$\mathbf{B} = \mathbf{U} p(z^{-1}) \begin{bmatrix} \mathbf{\Sigma} \\ \mathbf{0} \end{bmatrix} \mathbf{V}^{\mathrm{T}} \tag{77}$$

then

$$\tilde{\mathbf{P}} = \mathbf{U} p(z^{-1}) \left\{ \begin{bmatrix} \mathbf{\Sigma} \\ \mathbf{0} \end{bmatrix} + \mathbf{\Delta} \right\} \mathbf{V}^{\mathrm{T}} \tag{78}$$

where $\mathbf{E} = \mathbf{U}\mathbf{\Delta}\mathbf{V}^{\mathrm{T}}$ where $\mathbf{\Delta} \in \mathbb{R}^{m \times n}$ need not have any special structure.

The controllers in (30) can be written as

$$\mathbf{C}(z^{-1}) = \mathbf{V} \left[\Sigma^{-1}\mathbf{D} \ \mathbf{0} \right] c(z^{-1}) \mathbf{U}^{\mathrm{T}} \tag{79}$$

where $\mathbf{D} \in \mathbb{R}^{N \times N}$ is the diagonal matrix of controller gains. The actual open loop transfer function is

$$\begin{aligned} \mathbf{L}(z^{-1}) &= \tilde{\mathbf{P}}(z^{-1}) \mathbf{C}(z^{-1}) && (80) \\ &= \mathbf{U} p(z^{-1}) \left\{ \begin{bmatrix} \mathbf{\Sigma} \\ \mathbf{0} \end{bmatrix} + \mathbf{\Delta} \right\} \mathbf{V}^{\mathrm{T}} \mathbf{V} \left[\Sigma^{-1}\mathbf{D} \ \ \mathbf{0} \right] c(z^{-1}) \mathbf{U}^{\mathrm{T}} && (81) \\ &= \mathbf{U} p(z^{-1}) c(z^{-1}) \left\{ \begin{bmatrix} \mathbf{D} & \mathbf{0} \\ \mathbf{0} & \mathbf{0} \end{bmatrix} + \left[\mathbf{\Delta}\Sigma^{-1}\mathbf{D} \ \ \mathbf{0} \right] \right\} \mathbf{U}^{\mathrm{T}} && (82) \end{aligned}$$

There exists a matrix $\mathbf{X}$ such that [3, 4],

$$\mathbf{X} \left\{ \begin{bmatrix} \mathbf{D} & \mathbf{0} \\ \mathbf{0} & \mathbf{0} \end{bmatrix} + \left[\mathbf{\Delta}\Sigma^{-1}\mathbf{D} \ \ \mathbf{0} \right] \right\} \mathbf{X}^{-1} = \tilde{\mathbf{D}} \tag{83}$$

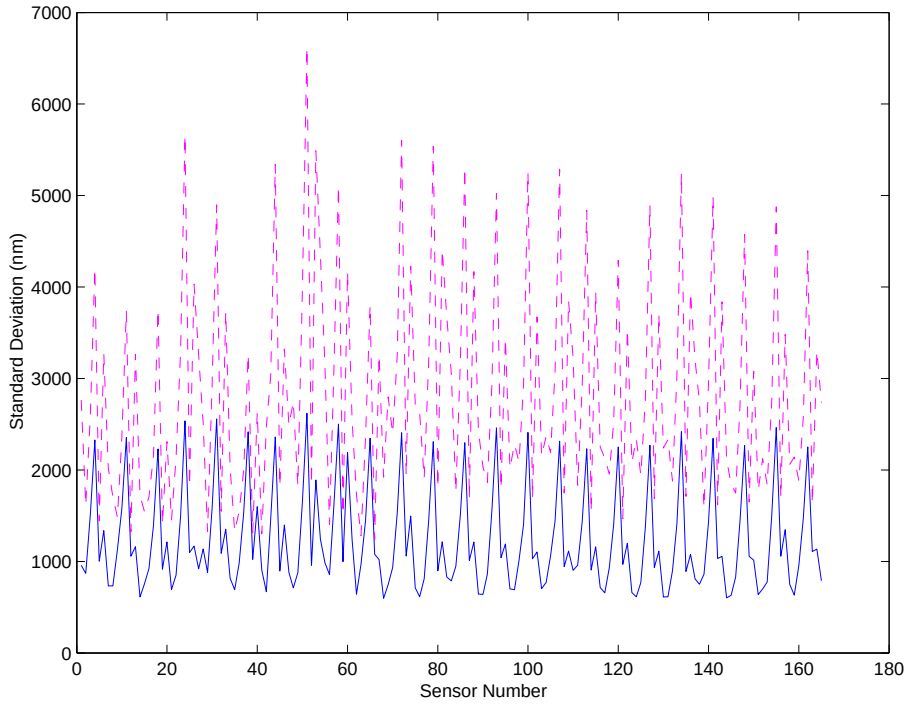


Figure 21: Standard deviation of controlled (blue line) and uncontrolled (magenta dashed line) variations plotted against sensor number

where $\tilde{\mathbf{D}} = \text{diag}\{\tilde{d}_m\}$, with $\tilde{d}_m \in \mathbb{C}$ being the eigenvalues of the matrix $\tilde{\mathbf{B}}\mathbf{C}$, so that

$$\mathbf{L}(z^{-1}) = \mathbf{U}\mathbf{X}\ \text{diag}\left\{\tilde{d}_m p(z^{-1})c(z^{-1})\right\}\ \mathbf{X}^{-1}\mathbf{U}^{\mathrm{T}} \tag{84}$$

Each mode of the perturbed system has the same dynamics as the nominal system, but a different gain. Using the Gershgorin theorem for the unsymmetric perturbation of a symmetric matrix [3], the gains of each mode in the perturbed system, $\tilde{d}_m$, lie within the union of a set of circles of radius $\|\mathbf{\Delta}\Sigma^{-1}\mathbf{D}\|_2$, centred on each of the diagonal elements of

$$\begin{bmatrix} \mathbf{D} & \mathbf{0} \\ \mathbf{0} & \mathbf{0} \end{bmatrix} \tag{85}$$

namely the gains derived from the nominal model, $\{d_n : n = 1, 2, \ldots, N\}$ and 0. Hence the Nyquist plots for each mode of the perturbed system will lie within the union of circles of radius $\|\mathbf{\Delta}\Sigma^{-1}\mathbf{D}\|_2$ centred at each point on the Nyquist plots for the nominal system. Given that the nominal system is open loop stable, for robust stability we require that none of these circles encloses the $-1 + \mathrm{j}0$ point, which will be achieved if the Nyquist plot associated with the largest value of d_n/σ_n, does not pass within $\|\mathbf{\Delta}\Sigma^{-1}\mathbf{D}\|_2$ of this point. For the choice of d_n in (34), this is equivalent to requiring that the circles associated with the first mode, which is the mode with the largest gain, and the condition for robust stability in the presence of uncertainties in $\mathbf{B}$, reduces to requiring that

$$\min_{\omega}\left\{\left|1 + \frac{\sigma_1}{{\sigma_1}^2 + \mu} p(\mathrm{e}^{-\mathrm{j}\omega T})c(\mathrm{e}^{-\mathrm{j}\omega T})\right|\right\} > \|\mathbf{\Delta}\Sigma^{-1}\mathbf{D}\|_2 \tag{86}$$

References

[1] A. Oppenheim and R. Schafer, *Discrete-Time Signal Processing.* Englewood Cliffs, NJ: Prentice Hall, 1989.

[2] R. Bracewell, *The Fourier Transform and its Applications*, 2nd ed. New York, NY: McGraw Hill, 1986.

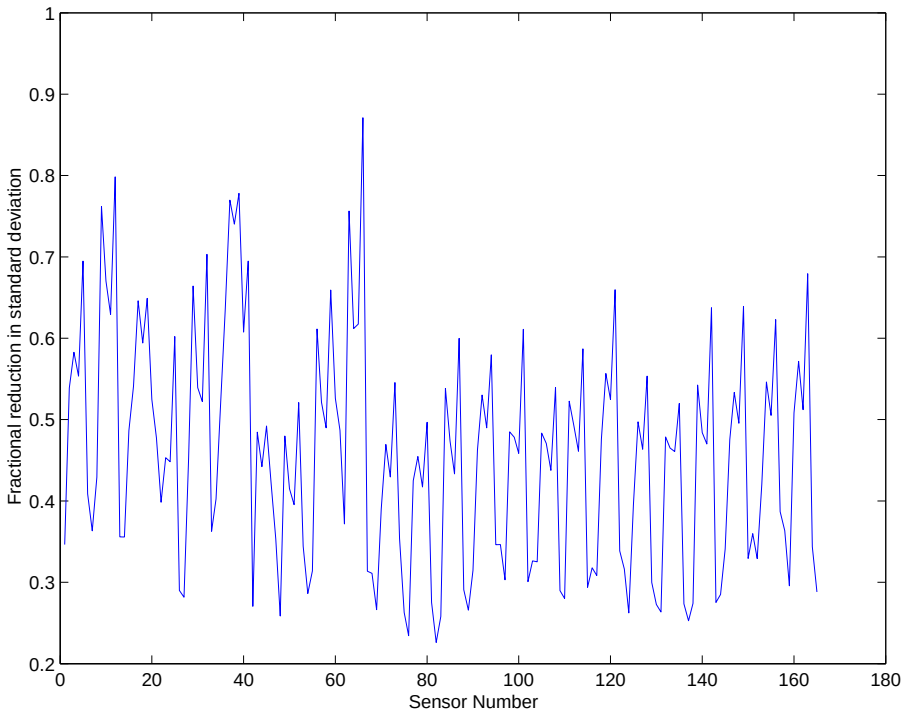


Figure 22: Fractional reduction in standard deviation achieved by the controller plotted against sensor number

[3] J. Wilkinson, *The Algebraic Eigenvalue Problem.* Oxford, UK: Clarendon Press, 1967.

[4] G. Golub and C. van Loan, *Matrix Computations*, 3rd ed. Baltimore, MD: John Hopkins University Press, 1996.

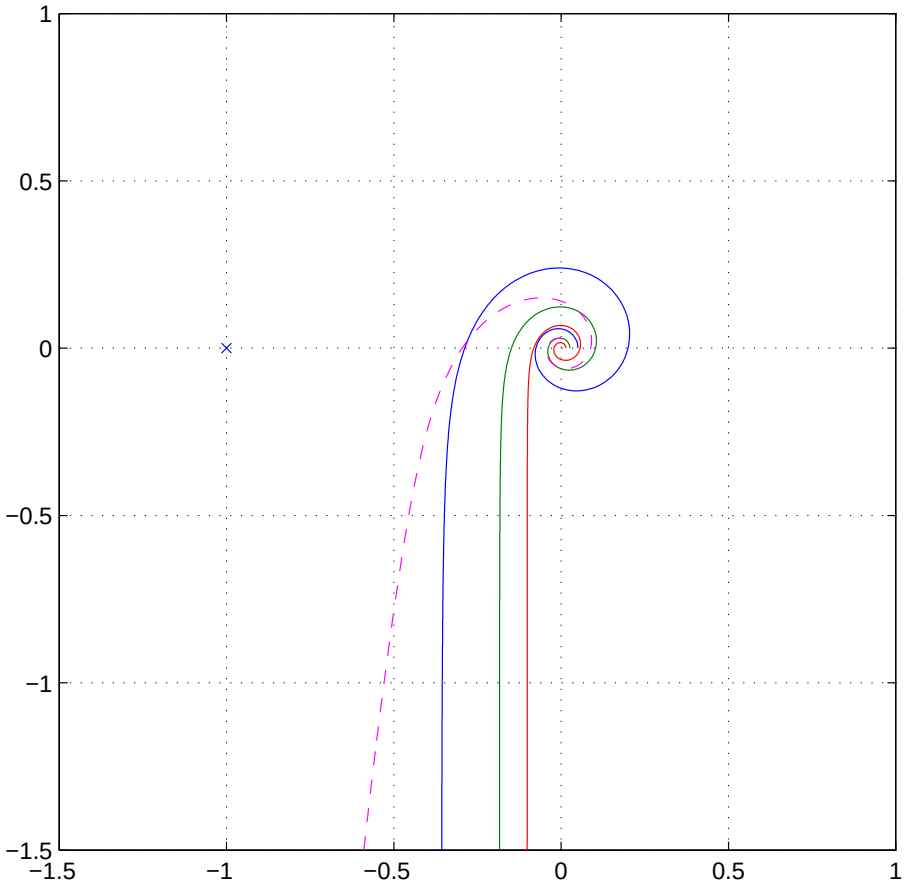


Figure 23: Nyquist plot of open loop transfer function $\ell_n(z^{-1})$ for three modes: $n = 1$ (blue solid line); $n = 5$ (green solid line) and $n = 10$ (red solid line), together with response of PI controller (magenta dashed line)